EPJdirect A1, 1–11 (2003)
DOI 10.1007/s1010503a123

EPJdirect
electronic only

ALICE Physics Reach

C. Blume[1]
for the ALICE collaboration

Institut für Kernphysik,
Johann Wolfgang Goethe Universität Frankfurt,
D-60486 Frankfurt, Germany
e-mail: blume@ikf.uni-frankfurt.de

Received:

Abstract. The ALICE experiment at the CERN LHC will be dedicated to the investigation of heavy ion reactions at the highest energies. The main objective is the study of strongly interacting matter under extreme conditions. The performance of the ALICE detector for a variety of observables are discussed. A special emphasis is put on the measurement of hard probes, which will be of high relevance at LHC energies. For all these observables p+p reactions will provide an important baseline measurement, so therefore p+p physics will be an integral part of the ALICE programme.

PACS: 12.38.Mh; 25.75.Nq

1 ALICE Physics

1.1 Strongly Interacting Matter

The main motivation for investigating nuclear matter at very high energies is to explore the phase diagram of strongly interacting matter [1]. From QCD predictions one expects a phase transition from normal hadronic matter to a different state of matter, the so-called Quark Gluon Plasma (QGP). In this plasma phase quarks and gluons, normally confined inside of hadrons, are quasi-free particles which can roam around freely over an extended volume. The chiral symmetry of the QCD Lagrangian, which is spontanously broken in hadronic matter, is restored in the QGP phase, i.e. the quarks will be effectively massless. Since the description of the QGP phase transition is in the realm of non-pertubative QCD, the only way of accessing its physics with the QCD from first principles is by studying the theory regularized on the lattice. Figure 1 shows as a result of such a calculation the energy density (ϵ/T^4) as a function of the temperature T [2]. Even though the result depends on the number of quark flavours considered, a significant jump in the energy density at a critical temperature of $T_c = 173 \pm 15$ MeV as a consequence of the phase transition is predicted. While the deposited energy at SPS and RHIC is probably enough to cross the phase boundary to the QGP phase and to establish it existence, at the LHC there will be the unique opportunity to study it quantitatively under clean conditions.

Figure 2 shows the phase diagram of strongly interacting matter in the T-μ_B-plane.. The band labelled "Lattice QCD" displays the phase boundary between a hadron gas and the quark gluon plasma as it is expected from lattice-QCD

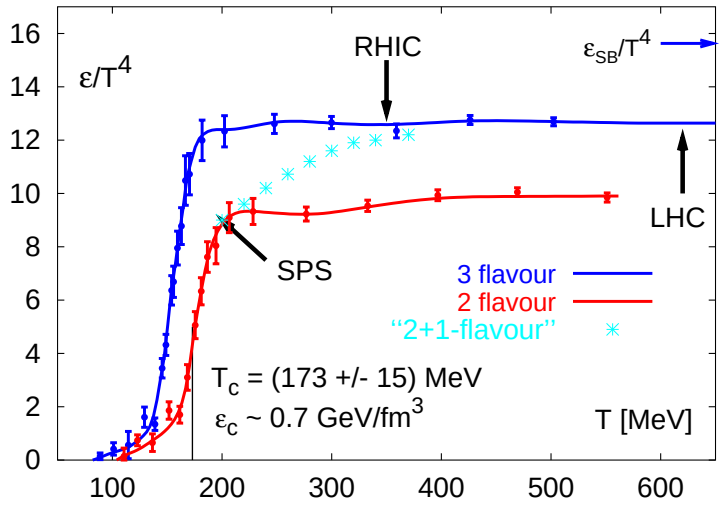

Fig. 1. Energy density as a function of the temperature for different numbers of degenerate quark flavours. The curves are the result of a lattice QCD calculation using improved gauge and staggered fermion actions [2].

calculations [3]. The points represent the temperature and baryonic chemical potential of the system at the point of chemical freeze-out, i.e. at the late stage of the reaction where inelastic reactions cease. These points have been derived from the analysis of the particle abundancies with a hadron gas model (e.g. [4, 5]). At SPS and RHIC the freeze-out conditions are already very close to the phase boundary, demonstrating that the system most likely has reached the deconfined phase before. When the beam energy is increased, the baryonic chemical potential is more and more approaching zero. At LHC energies one expects to create a QGP at $\mu_{\mathrm{B}} \approx 0$ with a very high initial temperature. The evolution of the created system will therefore closely follow the evolution of matter in the early universe. At LHC a central Pb+Pb collision will create energy densities of up to $\epsilon \approx 1000$ GeV/fm^3 [6]. Under these conditions the properties of the created matter will be qualitatively different compared to what is achievable at SPS and RHIC:

- The QGP matter will be dominated by low-x partons. Due to the saturated gluon densities a description via QCD with classical fields might be possible, since the saturation scale depends on the size of the nucleus: $Q_{\mathrm{S}} \propto A^{1/3}/x^{\delta}$, with $\delta \approx 0.3$ at HERA energies [8].
- The evolution of the system will spend most of its lifetime in the partonic phase. Therefore the observable collective effects will be dominated by the properties of the deconfined matter.
- Hard processes, which probe the initial phase of the reaction and are treatable with pertubative QCD will contribute to a significant part of the cross section.

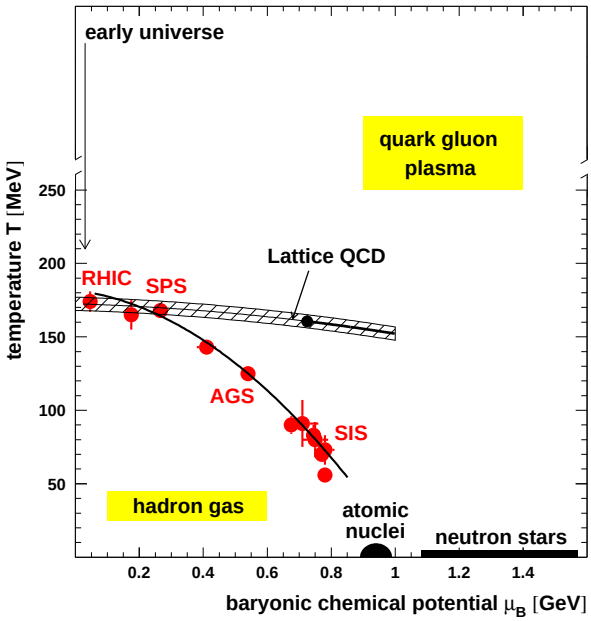

Fig. 2. The phase diagram of strongly interacting matter.

1.2 Observables

Generally speaking, one might divide the observables relevant in ultrarelativistic heavy ion collisions into three regimes:

"Soft" Regime: This covers the p_t-region of about 0-2 GeV/c and is clearly characterized by non-pertubative physics. The observables probe the very late stage of the reaction and the most important ones are:

- The particle yields in the low p_t-region provides information on the properties of the reaction at the chemical freeze-out.
- With the help of particle interferometry (e.g. pion-HBT) the thermal freeze-out conditions and the space-time evolution of the system can be investigated.
- The expansion dynamics of the reaction is reflected by collective effects like transverse flow.

"Semi-hard" Regime: In the region of intermediate p_t (2 - 5/10 GeV/c) hard processes start to contribute to the cross section. The observables are sensitive to earlier times of the reaction and smaller distance scales.

- The thermal evolution of the system can be probed by the measurement of thermal photons.

- The production of J/Ψ and open charm at these energies is determined by an interplay of hard processes, as well as a possible contribution from soft, thermal reactions. The J/Ψ is additionally affected by Debye screening effects in the plasma.
- The p_{t}-spectra in this region will be dominated by the presence of mini-jets.

"Hard" Regime: Above $p_{\mathrm{t}} = 10$ GeV/c processes that can be calculated via pertubative QCD and probe the very early state of the reaction are the main contribution. These are hard photons, open beauty, Υ, and jets. They will for the first time be measurable in heavy ion reactions at the LHC and therefore they will be given special attention in this article.

With ALICE it will be possible to detect the observables from all three regimes in a single detector, going from the hard (partonic) probes of the early stage to the soft (hadronic) probes of the late stage. This will offer the unique possibility of correlations between the hard and soft physics regimes.

1.3 p+p and p+A Physics

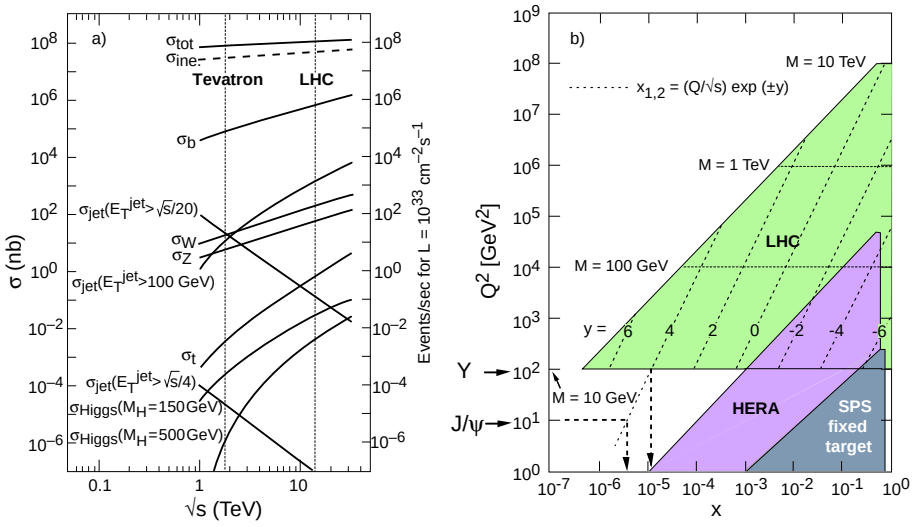

Fig. 3. On the left hand side the dependence of various contributions to the total p+p cross section are shown. The plot on the right hand side displays the region of Q^2 versus x, accessible in p+p collisions at the LHC.

Almost any observable measured in A+A collisions needs to be compared to its equivalent in p+p reactions in order to disentangle effects characteristic for deconfined nuclear matter from a mere superposition of elementary nucleon-nucleon reactions. This is especially true in the case of hard probes, such as

thermal photons, J/Ψ and Υ, and jets. Therefore, the measurement of p+p collsions will provide a very important benchmark for the investigation of A+A reactions. Aside from this, the study of soft physics in p+p reactions will be interesting on its own [9]. In p+p collisions at LHC energy densities of the order of $\epsilon \approx 1.2$ GeV/fm^3 will be achieved, which is comparable to the energy densities in nucleus-nucleus collsisions at SPS and RHIC, although restricted to a smaller volume. Even though hard processes constitute a significant part of the p+p cross section at LHC, the bulk of the cross section is still governed by soft and semi-hard physics (see Fig. 3). The investigation of this part of the cross section in the completely new energy regime of the LHC is therefore mandatory.

Similar arguments also hold for the measurement of p+A reactions. Apart from being important, as a kind of intermediate in system size between p+p and A+A, for the understanding of A+A collsions, the investigation of p+A will provide indispensible knowledge on the evolution of nuclear structure functions. Their determination will be neccessary for the interpretation of hard probes in A+A.

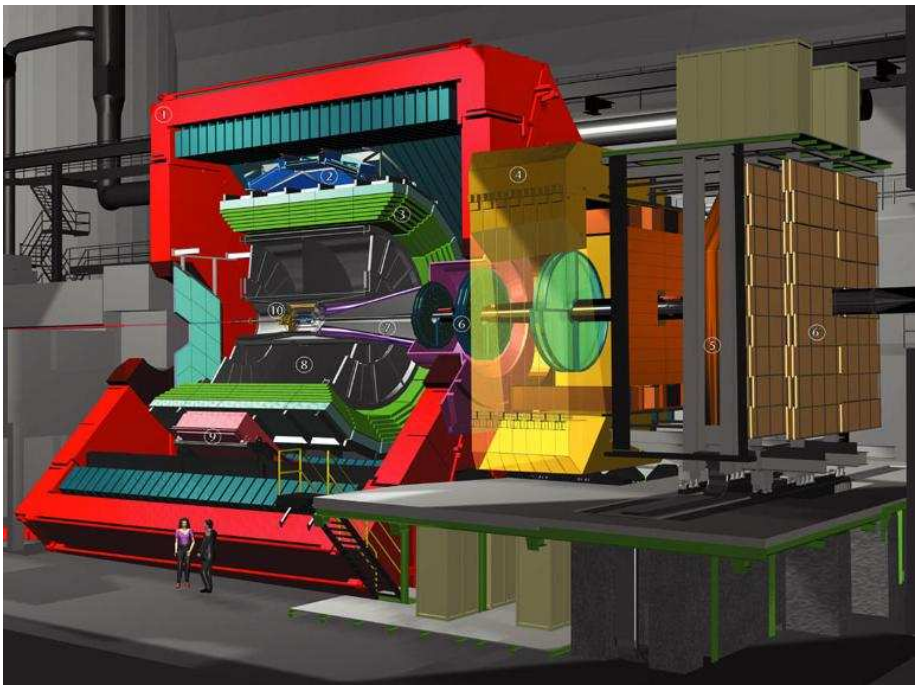

Fig. 4. The ALICE detector. Shown are the L3 magnet (1), the HMPID (2), the TRD and TOF (3), the MUON dipole magnet (4), the MUON tracking stations (5), the MUON trigger chambers (6), the absorber (7), the TPC (8), the PHOS detector (9), and the ITS (10).

2 The ALICE Experiment

2.1 Experimental Setup and Acceptance

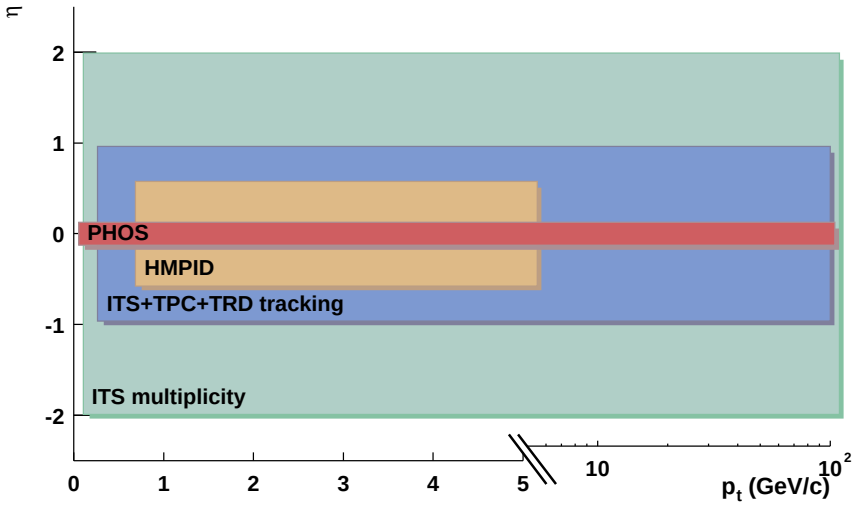

Fig. 5. The acceptance of the central detectors in the ALICE experiment.

Figure 4 shows the setup of the ALICE detector. The central barrel of the ALICE detector will be placed inside the L3 magnet and covers the acceptance region $|\eta| < 0.9$. Close to the interaction vertex there will be the Inner Tracking System (ITS). It is based on three different silicon detector types, arranged in six cylindrical layers with full azimuthal coverage. The main purpose is the determination of the position of the primary vertex and the tracking and particle identification of low momentum tracks. Going further outwards, there will be the Time Projection Chamber (TPC) as the main tracking device. It will also provide particle identification via a measurement of the energy loss in the detector gas. The TPC will be surrounded by the Transition Radiation Detector (TRD), whose task is the identification of electrons. Additionally, it serves as a triggering device on high-p_{t} tracks and will supplement the tracking. The next shell of the central barrel will consist of a layer of Time-Of-Flight detectors (TOF). They will complete the particle identification capabilities of ALICE in the central region. Details of this detector are discussed in [10]. The two outmost detectors of the central ALICE part, the High Momentum Particle Identification Detector (HMPID) and the PHOton Spectrometer (PHOS), will cover only part of the central acceptance. The HMPID is using the RICH technology to provide particle identification in the higher momentum range. The PHOS detector as an electromagnetic calorimeter will provide a measurement of photons and neutral mesons (π^0, η). Apart from the central detectors the ALICE experiment will also

include a muon arm (MUON) for the detection of muon pair in the pseudorapidity region $2.5 < \eta < 4.0$. A description of the setup an the physics capabilities of this detector is given in [11]. The design and the status of all ALICE detector components is also discussed in detail in [12].

Figure 5 summarizes the acceptance of the central ALICE detectors. The combination of ITS, TPC, and TRD will allow tracking in the range $|\eta| < 0.9$, starting with very low transverse momenta (≈ 100 MeV/c) up to very high p_t of ≈ 100 GeV/c. Also photon measurements will be possible in a similar momentum range, however, with much narrower η-acceptance.

2.2 Running Conditions for Pb+Pb and p+p Running

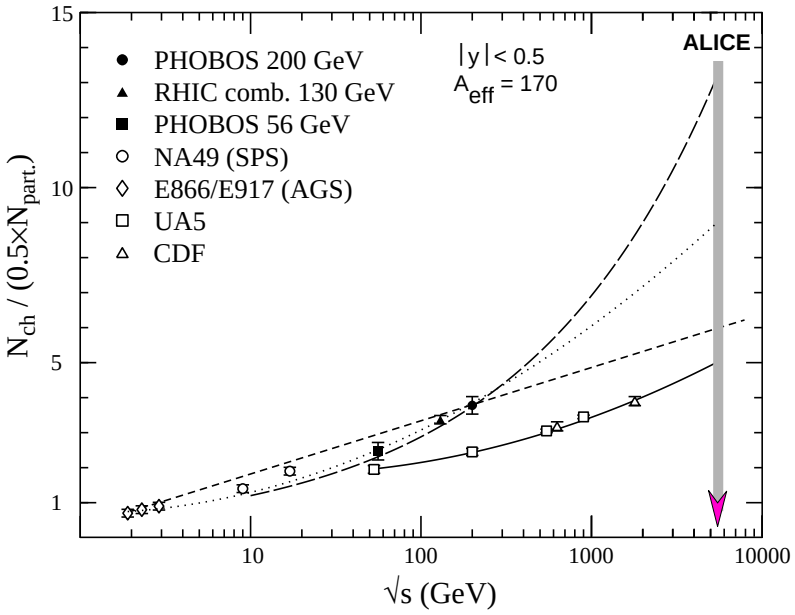

Fig. 6. The charged particle rapidity density per participant pair as a function of the center-of-mass energy for A+A and p+p collisions. The curves are explained in the text.

Nucleus-Nucleus collisions at LHC energies ($\sqrt{s_{\rm NN}} = 5.5$ TeV) are characterized by their extremely large particle multiplicity, which the detector must be able to resolve. However, even though there are now data from the RHIC experiments available, the lever arm between the RHIC energies and LHC is still too long to make any reliable predictions. This is evident from Fig. 6, which compiles the available data on the charged rapidity densities from A+A and p+p data. The solid line is a parametrization of the $\sqrt{s}$ dependence of the p+p points ($\approx 0.049 \ln^2(\sqrt{s}) + 0.046 \ln(\sqrt{s}) + 0.96$). The short dashed line is a fit to the nuclear data with $0.68 \ln(\sqrt{s}/0.68)$, while the dotted line is a fit with

$0.7 + 0.028 \ln^2(s)$. The long dashed line is an extrapolation using a color saturation model [13]. In order to assure the neccessary detector performance and to leave some margin for higher than currently predicted particle multiplicities or worse than expected background conditions, the design is therefore based on a maximum charged rapidity density of $dN_{\rm ch}/d\eta|_{\eta=0} = 8000$. The luminosity in the case of Pb-running will be $\mathcal{L} = 1 \times 10^{27}{\rm cm}^{-2}{\rm s}^{-1}$. This will result in an event rate of 8000 minimum bias collisions per second, yielding, integrated over an ALICE running period of 10^6s/year, 10^9 interactions/year and $\approx 10^7$ triggered events/year. In addition to the trigger on the event centrality, ALICE has a number of other triggers to select signals with small cross sections, using the MUON, PHOS, and TRD detectors. In the case of p+p event the PIXEL detector can provide a multiplicity trigger. A further reduction of the trigger rate can be achieved with the help of the High Level Trigger (HLT), that will do an online event reconstruction, combining the information of several detectors.

In the case of p+p collisions ALICE will run at a relatively low luminosity of $\mathcal{L} = 2 - 5 \times 10^{30}{\rm cm}^{-2}{\rm s}^{-1}$. Due to the drift time of 88μs, the TPC will collect several events during its gating time (≈ 25 for $\mathcal{L} = 2 \times 10^{30}{\rm cm}^{-2}{\rm s}^{-1}$). This event pile-up, however, can be removed online with the help of the HLT, reducing the data volume by a factor 5. Additionally, short running periods with an "ultra-low" luminosity ($\mathcal{L} \approx 10^{29}{\rm cm}^{-2}{\rm s}^{-1}$) without event pile-up are foreseen.

2.3 Tracking Performance

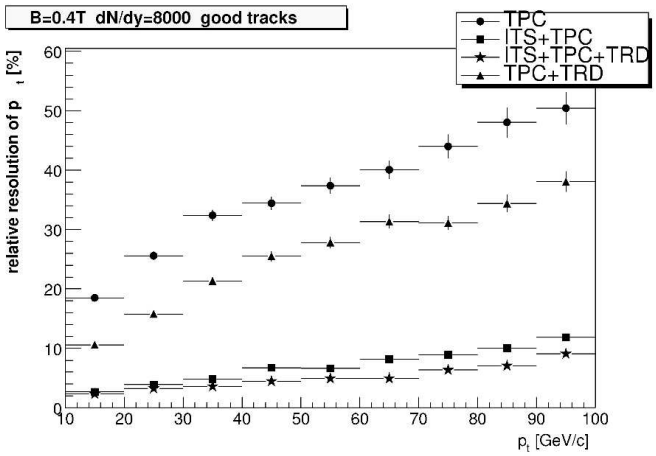

Fig. 7. The transverse momentum resolution as a function of $p_{\rm t}$ for different combinations of detectors.

Track reconstruction in the high multiplicity environment of central Pb+Pb reactions poses special demands on the detector performance, but also on the employed tracking algorithms. A lot of effort was invested recently, in order to optimize the Kalman filter based tracking in the central barrel to cope with the

high track densities. As a result, a reconstruction efficiency for tracks in the TPC of $\approx 98\%$ is achieved in simulated events. In these simulations a rapidity density of $dN_{\rm ch}/d\eta|_{\eta=0} = 8000$ and a magnetic field strenght of 0.4 T was assumed. Figure 7 shows the $p_{\rm t}$-resolution, derived from these simulations. By combining the tracking capabilities of all central tracking devices (ITS + TPC + TRD) a resolution of $\approx 9\%$ at a $p_{\rm t}$ of 100 GeV/c is possible. This will allow the study of high-$p_{\rm t}$ phenomena with very good accuracy and is therefore of high importance for the ALICE physics programme.

2.4 Particle Identification

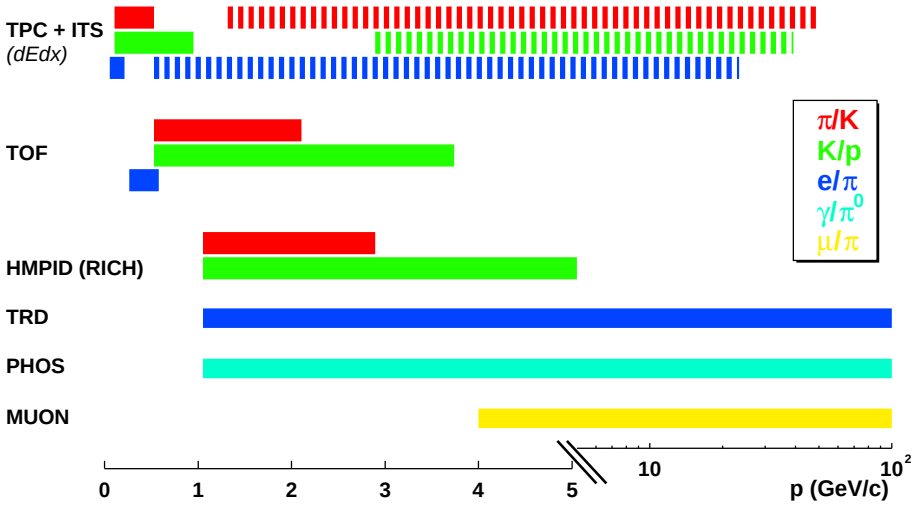

Fig. 8. Overview of the particle identification capabilities of the ALICE detector.

An unique feature of the ALICE detector is the possiblity to identify particle species over a very large region of momentum. These capabilities are summarized in Fig. 8. In the "low" momentum region particles can be identified via an energy loss measurement in the ITS and TPC. The TOF will separate π, K, p, and e in the "medium" momentum range (< 5 GeV/c). Due to a relatively good dE/dx-resolution in the TPC of $5.3 - 6.8\%$ (for $dN_{\rm ch}/d\eta|_{\eta=0} = 800$ and 8000, resp.), the energy loss measurement can, to a certain extend, also be employed in the region of the relativistic rise, thereby extending the accessible range to very high momenta (dashed lines in Fig. 8). In the "medium" to "higher" $p_{\rm t}$-range the identification will be supplemented by the HMPID, which will allow a precise particle type determination. The measurement of γ, π^0, and electrons will be possible for all momenta above 1 GeV/c.

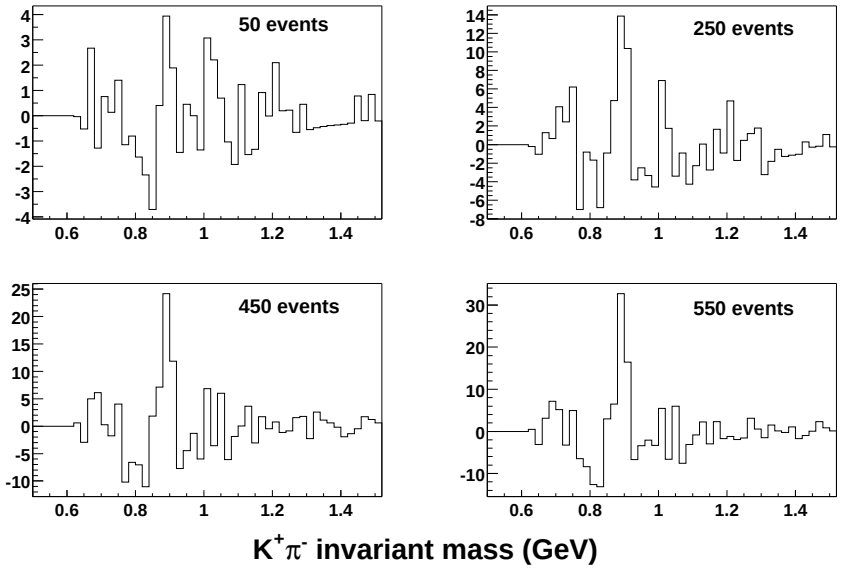

Fig. 9. The invariant mass distribution of K^+ and $\pi-$ pairs in central Pb+Pb reactions for different numbers of simulated events.

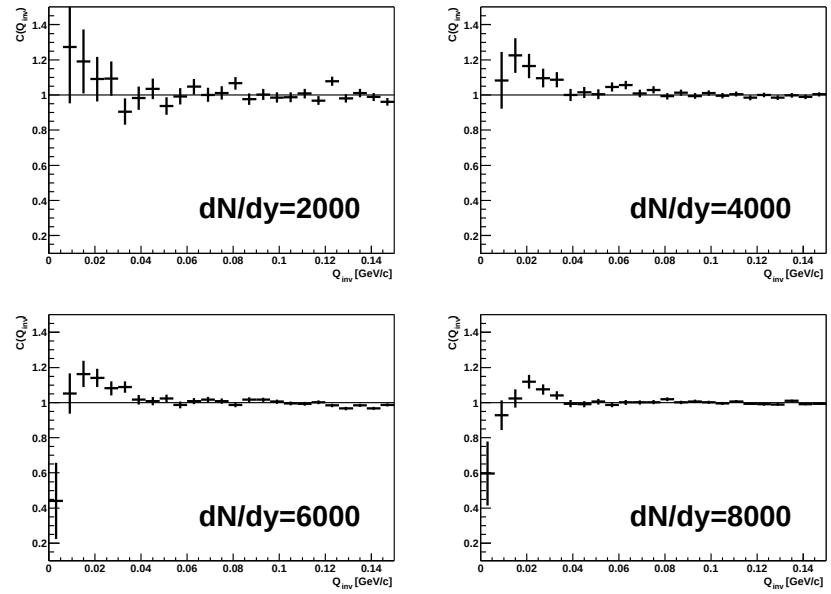

Fig. 10. The raw $\pi^+\pi^+$ correlation function derived from a single Pb+Pb event under different assumptions for the total event multiplicities.

3 Low p_t Physics Examples

The high multiplicity of produced particles in central Pb+Pb reactions at $\sqrt{s_{NN}} = 5.5$ TeV will allow the precise measurement of any soft physics observable already with relatively low statistics. This is illustrated in Fig. 9, showing the expected K(892)-resonance signal, measured via the decay K(892) $\rightarrow$ $K^+ \pi^-$, for different numbers of analysed events. Even after just 50 events an indication of a signal is visible, which is already quite prominent after 550 events.

Another opportunity offered by the high particle multiplicities is the possibility to study the fireball size via HBT interferometry on an event-by-event basis. Fig. 10 shows the $\pi^+\pi^+$ correlation signal, uncorrected for the Coulomb effect, achievable in a single event. A significant correlation is observable assuming a rapidity density of $dN/dy = 4000$.

4 Heavy Quarks

4.1 Open Charm

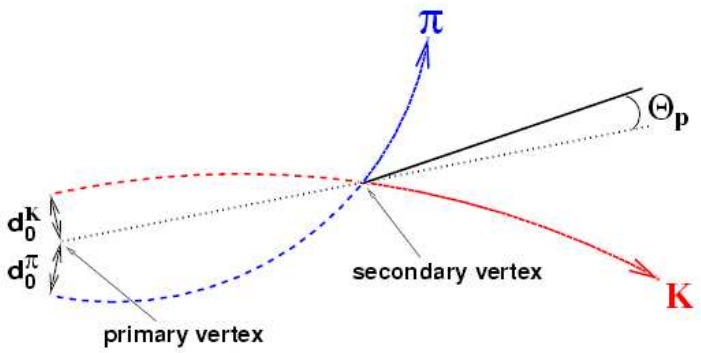

Fig. 11. Sketch of a D^0 decay into pion and kaon. The impact parameter of the pion and kaon track at the interaction vertex are d_0^π and d_0^K. θ_P ist the pointing angle of the D^0.

On one side the direct measurement of heavy flavours will be mandatory at LHC energies in order to provide a benchmark for any suppression or enhancement effects of quarkonia. On the other side, heavy quarks are probing the whole evolution of the QGP phase, since they are produced pertubatively in the early stages, but also thermally in later stages.

Experimentally, tagging on the impact parameter of the decay tracks is a powerful tool for measuring open charm and open beauty. As an example Fig. 11 shows the decay $D^0 \rightarrow K + \pi$ ($c\tau = 123.7$ fm). By cutting on the impact parameter distributions (d_0^π and d_0^K) tracks from D^0 decays can be selected.

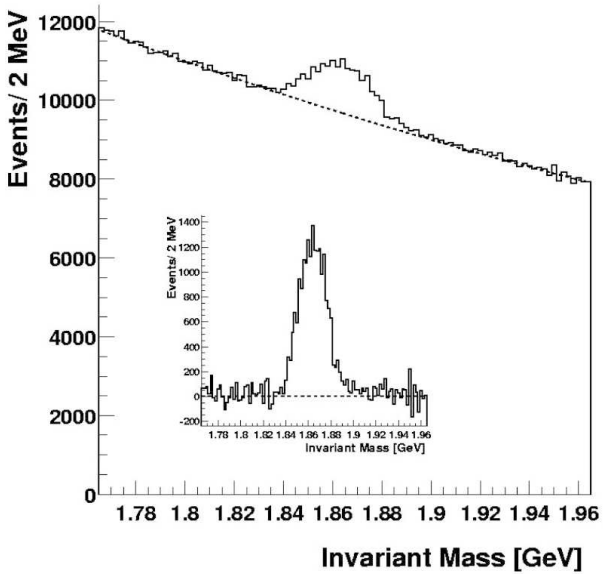

Fig. 12. The expected D^0 signal for central Pb+Pb reactions after one ALICE running year.

Additionally, a cut on the pointing angle θ_P of the reconstrcuted D^0 candidate relative to its flight path can be used to suppress combinatorial background.

With the help of this analysis strategy, a signal with a significance of 37 at a signal/background ratio of 11% can be extracted from central Pb+Pb reactions. The total expected signal for 10^7 events would be 13000 D^0. This simulation is based on PYTHIA 6 [14] for the $c\bar{c}$ production, tuned to NLO calculations [15] and using CTEQ4L as parton distribution function and EKS98 [16] to parametrize the nuclear shadowing. To this signal a backgound corresponding to the HIJING [17] event generator was added. The simulation is taking all know reconstruction effects into account [18]. The particle identification is done with the TOF detector. In the case of p+p collsions at $\sqrt{s} = 14TeV$ a significance of 84 and a signal/background ratio of 50% is expected. The total signal amounts to 20000 D^0 for 10^9 minimum bias p+p events.

Figure 13 show the corresponding p_t-spectra. In Pb+Pb the significance will be high enough at p_t down to 1 GeV/c and up to $p_t \approx 14$ GeV/c. In p+p a measurement even down to $p_t = 0$ GeV/c will be possible.

4.2 Open Beauty

Impact parameter tagging will also be important for the identification of semileptonic B decays. Figure 14 displays the d_0-distributions of electron tracks from different sources. The electron identification is done with the TPC and TRD detectors. While the contribution from background electrons (conversions) and from misidentified pions is concentrated at rather small impact parameter ($d_0 <$

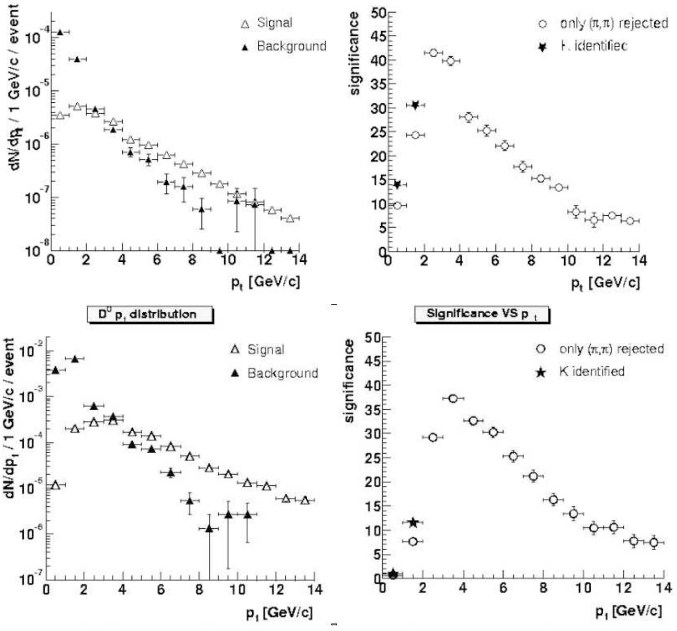

Fig. 13. The plots on the left hand side show the D^0 dN/dp_t for minimum bias p+p (upper) and central Pb+Pb (lower). On the right hand side the corresponding significance ($S/\sqrt{S+B}$) as a function of p_t is displayed.

$200 - 300\mu$m), the electrons from the decay $B \rightarrow e^- + X$ have a much flatter d_0-distribution. By choosing a cut at $d_0 = 150$ μm, B-decays can be cleanly isolated. For $p_t > 2$ GeV/c a signal/background ratio of 90% is achieved, with in total $5 - 10 \times 10^4$ signal electrons collected for 10^7 central Pb+Pb reactions.

4.3 Quarkonia Family

Measuring quarkonia will play a decisive role in heavy ion physics at the LHC. Since their binding energy is in the range of the mean energy of the QGP phase they are sensitive to screening effects that modify the $q\bar{q}$-potential. It is therefore essential to measure the whole family of quarkonia (J/Ψ, Ψ', Υ, Υ', Υ'') since their relative yield will allow to draw conclusions on the thermal development of the deconfined phase. At forward rapidities the MUON arm will detect all quarkonia via the di-muon channel [11]. In the central region their measurement will be possible with the combination of ITS+TPC+TRD via the di-electron channel. Figure 15 shows the acceptance in the latter case for J/Ψ and Υ, it extends down to $p_t = 0$ GeV/c. The expected mass resolution in the Υ mass region is 100 MeV for a magnetic field strength of 0.4T.

Since B mesons decay with a branching fraction of $\approx 1\%$ into J/Ψ, they will provide a substantial contribution to the totally observable J/Ψ signal. Via impact parameter tagging it will be possible to disentangle the contribution

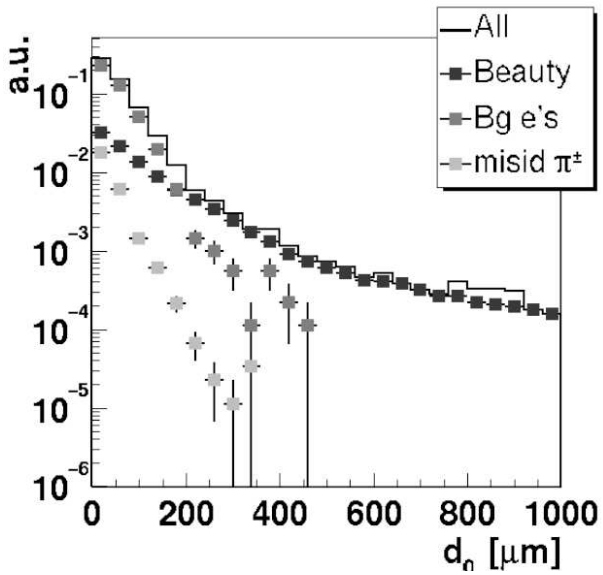

Fig. 14. The distribution of the impact parameter d_0 for electron tracks from different sources for central Pb+Pb events.

of these secondary J/Ψ from the primary ones. This is illustrated in Fig. 16, where the different impact parameter distributions of J/Ψ from B decays and of primary J/Ψ are compared. This will provide an alternative way of measuring the B meson yield.

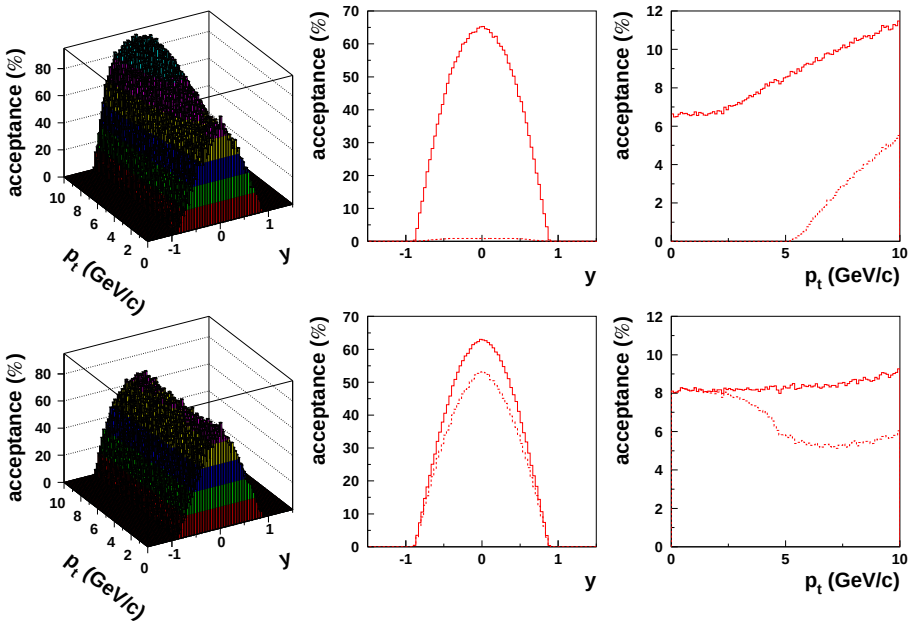

Fig. 15. The acceptance for J/Ψ (upper row) and Υ (lower row) as a function of p_t and rapidity y. The middle and the right plots show the acceptance with (dashed line) and without (solid line) the trigger cut on single electron p_t.

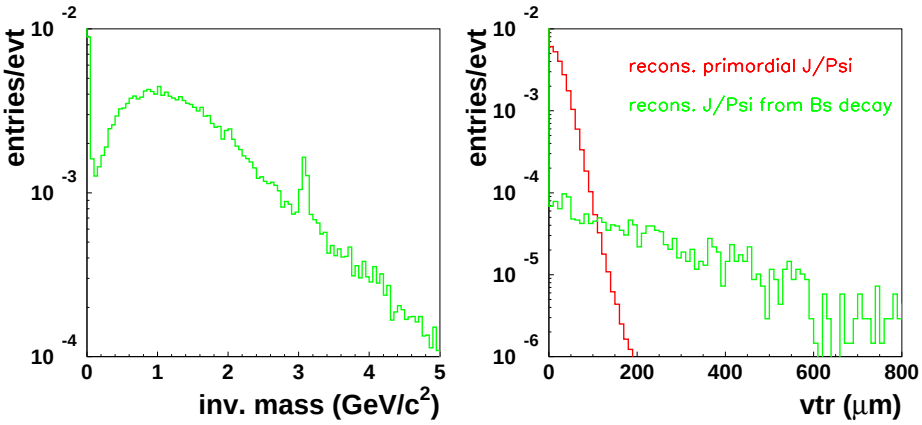

Fig. 16. Invariant mass distribution of e^+e^- pairs with displaced vertices (left panel) and the impact parameter distribution for pairs in the J/Ψ mass region (right panel).

5 Parton Energy Loss

5.1 High p_t Particle Spectra

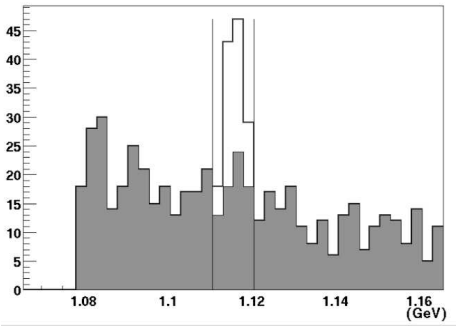

Fig. 17. The invariant mass distribution of $p\pi^-$ pairs.

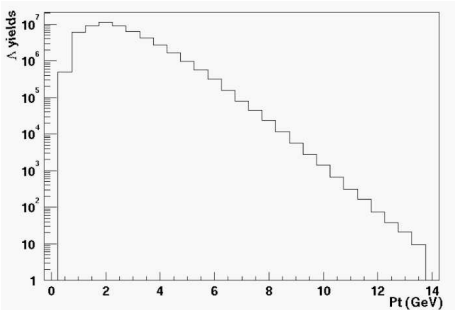

Fig. 18. The reconstructed Λ p_t-spectrum for 10^7 central Pb+Pb events.

A parton, scattered off in one of the hard collision in the inital phase of the A+A reaction, will radiate gluons when traversing the surrounding nuclear medium. This gluon radiation depends on the path length inside the medium and it is expected to be stronger in a deconfined medium. The observable effects would be:

- Reduction of the inclusive particle spectra at high p_t.
- Suppression of mini-jets.
- Change of the fragmentation function of hard jets ($p_t \gg 10$ GeV/c).

A strong indications for presence of these effects are suggested by the recent results from the RHIC accelerator [19]. Since the effect on the inclusive particle spectra is expected to be flavour specific, it requires therefore the measurement of identified hadrons (π, K, p, Λ) at high p_t. As an example for the ALICE capabilities, Fig.18 shows the reconstructed Λ p_t-spectrum, as it would be measurable with 10^7 central Pb+Pb events. Figure 17 shows the corresponding Λ signal after 10 events, with a signal/background ratio of 1. The number of expected Λ/event of 5.5 can still be improved by applying particle identification on the daughter tracks, but already this simplified analysis demonstrates that p_t up to 12 GeV/c will easily be accessible.

The PHOS detector will allow to measure γ and π^0 up to very high p_t. Figure 19 shows the expected γ p_t-spectrum for 10^7 central Pb+Pb events, while Fig. 20 shows the accessible region if a trigger on high-p_t photons is used. A separation of direct γ and π^0 will be possible up $p_t \approx 100$ GeV/c. For lower p_t ($< 30 - 40$ GeV/c) the separation is based on statistical methods, while for higher p_t it will be possible on an event-by-event basis.

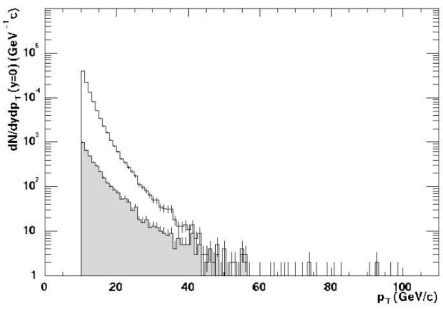

Fig. 19. The inclusive γ $p_{\rm t}$-spectrum for 10^7 central Pb+Pb events without high-$p_{\rm t}$ trigger. The shaded histogram represent the direkt γ, while the other one consists of the sum of direkt and dacay γ.

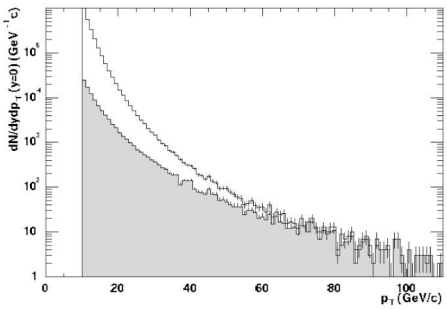

Fig. 20. The inclusive γ $p_{\rm t}$-spectrum for 10^7 central Pb+Pb events with a high-$p_{\rm t}$ trigger.

5.2 Jets via Correlations

A statistical way of studying jets is to analyze correlations relative to given leading particles. These leading particles are defined as exceeding a threshold in transverse momentum $p_{\rm t}$(seed). By combining them with all other particles above a lower $p_{\rm t}$ threshold than $p_{\rm t}$(seed) a correlation radius in η-ϕ space can be calculated: $R = \sqrt{\eta^2 + \phi^2}$. Thus, a $d^2N/d\phi d\eta$ distribution is transformed into a $1/RdN/dR$ distribution. Figure 21 shows such a distribution as a result of a simulation that is based on 1000 HIJING events, produced with default settings [17]. As Fig. 22 demonstrates there is a clear difference between the $p_{\rm t}$-distributions of particles with small R and thereby with a high propability of belonging to the original jet-cone compared to those with a R larger than 1. This will allow to qualitatively analyse changes in the jet fragmentation by performing this analysis e.g. as a function of the system size.

Another approach is to study the two particle correlation function:

$$C(\alpha) = \frac{dN/d\alpha(\text{real})}{dN/d\alpha(\text{mixed})} \text{ with } \alpha = \arccos\left(\frac{\mathbf{p}_1 \cdot \mathbf{p}_2}{|\mathbf{p}_1||\mathbf{p}_2|}\right)$$

The result of the correlation from simulated Pb+Pb events is presented in Fig 23. A clear increase of the correlation strength with increasing $p_{\rm t}$ is visible, demonstrating the sensitivity of the method to the effects induced by the emission of mini-jets.

Beyond these statistical methods of studying changes in the jet fragmentation, the direct measurement of jets will be feasible in heavy ion reactions at LHC energies. Of great importance in this context would be the proposed addition of an electromagnetic calorimeter (EMCAL)[20] to the ALICE setup.

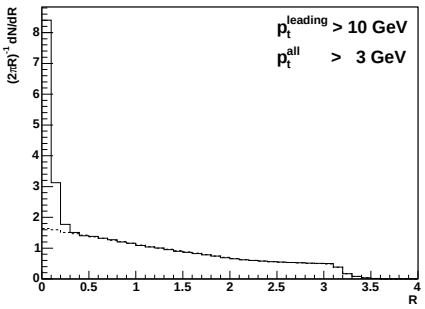

Fig. 21. The distribution of the correlation radii R relative to a leading particle with $p_t(\text{seed}) > 10$ GeV/c. All particles with $p_t > 3$ GeV/c are included.

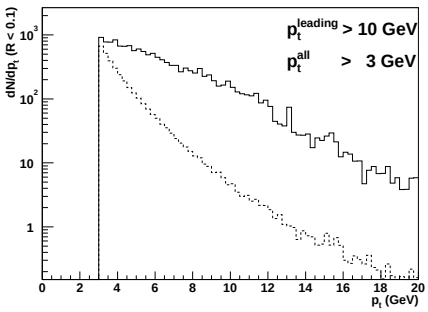

Fig. 22. The p_t-distribution of particles with a correlation radius $R < 0.1$ and $1 < R < 2$.

6 Conclusions

The ALICE experiment will provide access to effectively all observables relevant for heavy ion physics at LHC energies, ranging from the low p_t region (> 0.1 GeV/c) up to very high p_t of ≈ 100 GeV/c. The observables will include soft physics observables as yields of identified particles, correlations, event-by-event observables, and flow, as well as observables from the hard physics regime: Heavy quarks, quarkonia, photon, and jets. Additionally, p+p and p+A measurements will play a decisive role in order to define a baseline for A+A observables on the one hand, but will also be an important part of the ALICE physics programme on it own on the other hand. The physics performance report [6], that is currently being compiled, will summarize the physics capabilities for all projected observables of the ALICE experiment.

7 Acknowledgements

I would like to acknowledge the many contributions from and helpful discussions with my colleagues from the ALICE collaboration who helped me in preparing this contribution.

References

1. For a recent overview see: Proceedings of the 16th International Conference on Ultra-Relativistic Nucleus-Nucleus Collisions, Quark Matter 2002, eds: H. Gutbrod, J. Aichelin, and K. Werner, Nucl. Phys. **A715** (2003).
2. F. Karsch, E. Laermann and A. Peikert, Phys. Lett. **B478** (2000) 447.
3. Z. Fodor and S.D. Katz, Nucl. Phys. **B106** (2002) 441.
4. P. Braun-Munzinger, I. Heppe, and J. Stachel, Phys. Lett. **B465** (1999) 15.

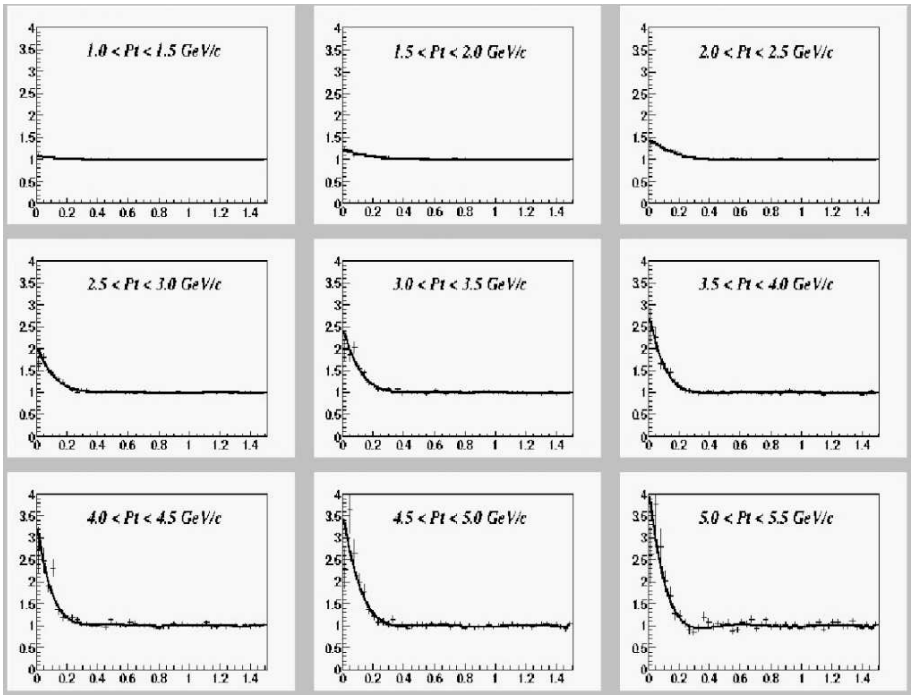

Fig. 23. The two particle correlation function $C(\alpha)$ (see text for a definition) in different regions of p_{t}.

5. P. Braun-Munzinger, D. Magestro, K. Redlich, and J. Stachel, Phys. Lett. **B518** (2001) 41.
6. *ALICE Physics Theoretical Overview*, ALICE Int. Note 2002-025, 16 Sept. 2002.
7. A. Krasnitz and R. Venugopalan, Nucl. Phys. **B557** (1999) 237.
8. K. Golec-Biernat and M. Wüsthoff, Phys. Rev. **D60** (1999) 114023.
9. J.P. Revol, ALICE-PUB-2002-02.
10. C. Williams, *ALICE: TOF system*, these proceedings.
11. A. Morsch, *ALICE: Muon spectrometer*, these proceedings.
12. Y. Schutz, *ALICE status*, these proceedings.
13. K.J. Eskola, K. Kajantie, P.V. Ruuskanen, and K. Tuominen, Nucl. Phys. **B570** (2000) 379.
14. T. Sjöstrand, P. Edén, C. Friberg, L. Lönnblad, G. Miu, S. Mrenna, and E. Norrbin, Computer Phys. Commun.**135** (2001) 238.
15. M. Mangano, P. Nason, and G. Ridolfi, Nucl. Phys. **B 373** (1992) 295.
16. K.J. Eskola, V.J. Kolhinen, and C.A. Salgado, Eur. Phys. J. **C9** (1999) 61.
17. X.N. Wang and M. Gyulassy, Phys. Rev. **D44** (1991) 3501.
18. A. Dainese, R. Turrisi, and N. Carrer, ALICE Int. Note 2002-05, 18. Feb. 2002.
19. G. Roland, *RHIC: Physics Results*, these proceedings.
20. T. Cormier, *Jet Physics in Alice and the Proposed New Electromagnetic Calorimeter*, these proceedings.